Effect of Coronal Fracture Angle on the Stability of Screw Fixation in Medial Malleolar Fractures: A Finite Element Analysis

Journal:	*Part H: Journal of Engineering in Medicine*
Manuscript ID	JOEIM-21-0339.R2
Manuscript Type:	Original article
Date Submitted by the Author:	n/a
Complete List of Authors:	EMRE, Tuluhan Yunus ; Biruni University, Orthopaedics and Traumatology CELIK, H. Kursat; Akdeniz University, Dept. of Agric. Machinery and Technology Engineering ARIK , Hasan O. ; Antalya Training and Research Hospital, Orthopaedics and Traumatology Rennie, Allan ; Lancaster University, Engineering Department KOSE, Ozkan ; Antalya Training and Research Hospital, Orthopaedics and Traumatology
Keywords:	Medial Malleolus Fracture, Fracture Angle, Fixation, Finite Element Analysis, Biomechanics
Abstract:	Malleolar screw fixation is the most widely used treatment method for medial malleolar (MM) fractures. Here, although buttress plate fixation is advocated for vertical MM fractures, the angular discrimination between oblique and vertical MM fractures is still not fully understood. The purpose of this study is to test the adequacy of screw fixation in MM fractures with different angles and determination of a 'critical fracture angle' to guide surgeons in the decision-making for screw fixation for MM fractures by utilising an advanced engineering simulation approach. In addition to loading of the healthy tibia structure, various cases of the MM fracture double screw fixation were considered in this research and their static loading conditions just after fixation operation were simulated through nonlinear (geometric and contact nonlinearity) finite element analysis (FEA). Minimum and maximum separation distances (gap) of 3.750 µm and 150.340 µm between fracture fragments at fracture angles of 30˚ and 90˚ were calculated respectively against minimum and maximum sliding distances of 25.869 µm and 41.372 µm between fracture fragments at fracture angles of 90˚ and 35˚ respectively. The FEA results revealed that while the separation distance was increasing, the sliding distance was decreasing and there were no distinct differences in sliding distances in the scenarios from fracture angles of 30° to 90°. it was interpreted that the FEA scenarios were setup in this study by utilising acceptable assumptions providing logical outputs under pre-defined boundary conditions. Finally, it was concluded that the screws fixed perpendicular to the fracture in a MM fracture with more than 70° angle with the tibial plafond results in a significant articular separation (>100 µm) during single-leg stand. Below this critical angle of 70°, two screws provide sufficient fixation.

Effect of Coronal Fracture Angle on the Stability of Screw Fixation in Medial Malleolar Fractures: A Finite Element Analysis

Tuluhan Yunus EMRE[1], H. Kursat CELIK[2]*, Hasan O. ARIK[3], Allan E.W. RENNIE[4], Ozkan KOSE[3]

[1] Orthopaedics and Traumatology Dept., Medical Faculty, Biruni University, Istanbul, Turkey
[2,] Dept. of Agr. Machinery and Technology Engineering, Akdeniz University, Antalya, Turkey*
[3] Orthopaedics and Traumatology Dept., Antalya Training and Research Hospital, Antalya, Turkey
[4] Engineering Dept., Lancaster University, Lancaster, United Kingdom

Corresponding author	*: Dr H. Kursat CELIK*
e-mail	*: hkcelik@akdeniz.edu.tr*
Tel	*: +90 242 310 65 70*
Fax	*: +90 242 310 24 79*
Address	*: Dept. of Agr. Machinery and Technology Engineering, Akdeniz University, 07070, Antalya, Turkey*

ABSTRACT

Malleolar screw fixation is the most widely used treatment method for medial malleolar (MM) fractures. Here, although buttress plate fixation is advocated for vertical MM fractures, the angular discrimination between oblique and vertical MM fractures is still not fully understood. The purpose of this study is to test the adequacy of screw fixation in MM fractures with different angles and determination of a ‘critical fracture angle’ to guide surgeons in the decision-making for screw fixation for MM fractures by utilising an advanced engineering simulation approach. In addition to loading of the healthy tibia structure, various cases of the MM fracture double screw fixation (14 simulation scenarios in total with fracture angles between 30° and 90°, in 5° increments) were considered in this research and their static loading conditions just after fixation operation were simulated through nonlinear (geometric and contact nonlinearity) finite element analysis (FEA). Patient-specific computed tomography scan data, parametric three-dimensional solid modelling and finite element method (FEM) based engineering codes were employed in order to simulate the fixation scenarios. Visual and numerical outputs for the deformation and stress distributions, separation and sliding behaviours of the MM fracture fragments of various screw fixations were clearly exhibited through FEA results. Minimum and maximum separation distances (gap) of 3.75 µm and 150.34 µm between fracture fragments at fracture angles of 30˚ and 90˚ were calculated respectively against minimum and maximum sliding distances of 25.87 µm and 41.37 µm between fracture fragments at fracture angles of 90˚ and 35˚ respectively. The FEA results revealed that while the separation distance was increasing, the sliding distance was decreasing and there were no distinct differences in sliding distances in the scenarios from fracture angles of 30° to 90°. The limitations and errors in a FEA study are inevitable, however, it was interpreted that the FEA scenarios were setup in this study by utilising acceptable assumptions providing logical outputs under pre-defined boundary conditions. Finally, the fracture healing threshold for separation and/or sliding distance between fracture fragments was assigned as 100 µm by referring to previous literature and it was concluded that the screws fixed perpendicular to the fracture in a MM fracture with more than 70° angle with the tibial plafond results in a significant articular separation (>100 µm) during single-leg stand. Below this critical angle of 70°, two screws provide sufficient fixation.

KEYWORDS: Medial Malleolus Fracture, Fracture Angle, Fixation, Finite Element Analysis, Biomechanics

[1] Tuluhan Yunus EMRE, MD, Assoc. Prof.	*drtuluhan@yahoo.com*	*ORCID: 0000-0003-3571-2836*
[2] H. Kursat CELIK, PhD, Assoc. Prof.	*hkcelik@akdeniz.edu.tr*	*ORCID: 0000-0001-8154-6993*
[3] Hasan O. ARIK, MD	*drhasanarik82@gmail.com*	*ORCID: 0000-0002-3407-9744*
[4] Allan E.W. RENNIE, PhD, Prof.	*a.rennie@lancaster.ac.uk*	*ORCID:0000-0003-4568-316X*
[3] Ozkan KOSE, MD, FEBOT, Assoc. Prof.	*drozkankose@hotmail.com*	*ORCID: 0000-0002-7679-9635*

Word Counts	: Approx. 6500 (Except abstract, references and acknowledge)
Number of Figures	: 4
Number of Tables	: 4
Supplementary	: 2

1. INTRODUCTION

Medial malleolar (MM) fractures are common injuries that can occur in isolation or in combination with lateral and posterior malleolar fractures. Population-based studies have reported that one in every four (25%) ankle fractures involve medial malleolus [1]. Treatment of MM fractures can be managed with either surgical fixation or conservative methods. Isolated stable MM fractures with less than 2 mm displacement can be treated conservatively with cast immobilisation. However, in unstable ankle fractures such as bi-malleolar and tri-malleolar fractures, surgical fixation of all fractures is usually advocated to restore ankle stability [2–4]. Surgical treatment of MM fractures should aim to obtain an anatomic reduction, keep the talus anatomically within the ankle mortise, and maintain this reduction until the bone union is achieved. The fixation should be stable enough to allow early postoperative rehabilitation, including ankle exercises and even total or partial weight-bearing [5,6]. In current ankle fracture classification systems, transverse, oblique, and vertical MM fractures are described, and specific fixation methods are proposed according to these fracture types [2,7,8]. K-wires and tension band wiring techniques are recommended for distal fractures with a small fragment. Transverse and oblique fractures are commonly fixed with two partially threaded cancellous lag screws inserted perpendicular to the fracture plane. Lag screws and/or buttress plates are recommended for vertical shear fractures to prevent vertical migration of the fracture [9]. However, the geometry of the fracture, size of the fragment, quality of the bone, and the severity of the soft tissue injury are all critical factors that determine the choice of surgical technique and implants [3,10]. The geometry of the MM fracture is closely related to the mechanism of the ankle injury. Lauge-Hansen (1950) demonstrated that a predictable sequence of injuries and fracture patterns occur on a particular foot position with a particular direction of deforming force [7]. In addition to the magnitude and the direction of the force, it is known that the quality of the bone and the strength of the ligaments influence the final geometry of the ankle fracture.

In current treatment recommendations, fracture pattern definitions are purely subjective and not based on angular measurements. In other words, there is no objective definition (angular measurement) about which fractures will be considered as an oblique MM fracture or a vertical MM fracture. The intra-observer and inter-rater reliability of the Herscovici MM fracture classification was examined by Aitken *et al* (2017) [11]. This study reported that the fracture type could not be decided in 26% of cases due to the obliquity of the fracture line. In previous biomechanical studies, it has been shown that buttress plate fixation provides a more stable construct as the fracture angle progresses from oblique to vertical pattern [12–14]. However, the critical fracture angle where the screw fixation would retain sufficient stability is unknown. The hypothesis of this study was, 'Two malleolar screws inserted perpendicular to the fracture line would be insufficient at a critical fracture angle under single stand weight-bearing loading.' This study aimed to test the adequacy of screw fixation in different fracture angles and determine a 'critical fracture angle' to guide the surgeons in the decision of implants/screw fixation for MM fractures utilising finite element analysis (FEA). Thus, a surgical decision on a plate versus screw fixation may be confidently performed on an objective assessment.

2. MATERIALS AND METHODS

2.1. Finite Element Analysis

Various cases of the MM fracture double screw fixation were considered in this research and their static loading conditions immediately following the fixation operation were simulated through Finite Element Method (FEM) based engineering simulation techniques with nonlinear contact definitions. In the simulation scenarios, in addition to loading of the healthy tibia structure (1 simulation), loading of the MM fracture fixation scenarios were simulated for various combinations of fracture angles between 30° and 90°. The division between fracture angles in the simulation scenarios was set up as 5° (13 simulations), thus 14 simulation scenarios were set up in total (one intact and 13 fracture simulations). Patient-specific computed tomography scan data was used as the reference for solid modelling procedures, which were finalised using SolidWorks 2019 parametric three-dimensional (3D) solid modelling software [15]. Static structural module of the ANSYS Workbench 2019.R2 commercial FEM code [16] was employed in order to simulate the scenarios. The list of the FEA scenarios is given in Table 1.

(**Table 1.** List of the FEA scenarios)

2.1.1. Geometric Model

The patient-specific healthy human ankle CT scan data was the reference for creating realistic CAD data used in this study. The scanning operation was conducted using the CT device (SOMATOM go.Up, Siemens, Munich, Germany) installed in Antalya Training and Research Hospital (Antalya-Turkey, with a slicing distance of 0.7 mm from 80 mm above the ankle joint down to the heel in the supine position (total of axial slices: 334; spatial resolution: 0.3 mm). The scan parameters were set to 130 KV and 42 mA. The patient was a 29 –year old male subject, 184 cm in height and 98 kg in weight without previous history of foot/ankle disease, congenital or acquired deformities or systemic disease. Written informed consent was obtained from the patient to use the imaging data anonymously.

The CT scan was reviewed by two experienced radiologists and one orthopaedic surgeon, and no osseous lesions were detected. Initially, CT scan data of the whole ankle joint was imported into 3D Slicer (v 4.10.2) software [17]. The segmentation procedure of soft tissue from bony parts was carried out via 3D Slicer segment editor tools using the following steps: importing CT scan data (DICOM file) (1); threshold-based segmentation operation (specific threshold range: 99/2210) (2); cropping and cleaning operations (3); 3D view tool and initial surface smoothing operation (kernel size: 5 mm – 19x19x7 pixels for tibia and kernel size: 2 mm – 7x7x3 pixels for talus) (4). Subsequently, the tibia and talus bones were extracted from the whole ankle 3D images, and then they were exported as separate stereolithography (STL) files. These files were subsequently imported into the Autodesk Meshmixer 2019 software [18] to perform final geometry cleaning and final surface smoothing operations. Finally, the processed geometric data of the bones were separately imported into SolidWorks software for solid model conversion, final model processing, fracture modelling and assembly operations. In the solid modelling operations, cortical and trabecular bones and cartilage areas of the tibia and talus bones were separately modelled and assembled according to CT scan 3D visuals. Measurements have been carried out on CT images and component separation was processed in the solid modelling software. The other components connected to the ankle joint (such as fibula bone, ligaments, muscles, other inner tissues and the skin) were not included in the FEA scenarios.

In addition to intact bone structure (no-fracture), 13 different MM fracture fixation solid models were created for the simulation scenarios. Various fracture angles between 30° and 90° were parametrically modelled. The fracture start point was assigned at the approximate fracture point/corner of the tibia medial malleolus section where the critical notch effect might be observed. Cortical bones, trabecular bones, cartilage and fixation screws (malleolar or cancellous screw) were separately modelled and assembled at the fracture fragments. Based on the original geometry data taken from the CT scan, it was observed that the thickness of the cortical bone is not uniformly distributed at the bone structures. The thickness of the cortical bone successfully separated from the trabecular bone through the solid modelling operation with a value varying between 0.98 mm and 3.33 mm (approximately). Similarly, cartilage areas were modelled based on CT scan images and provided complete surface contact visualisation for bone-to-cartilage and cartilage-to-cartilage; thus, non-uniform realistic cartilage thickness distribution was obtained. Average thickness values of the articular cartilage between tibia and talus bones varied between 0.52 mm and 2.85 mm in the modelling operation. The cartilage contact surface area between tibia and talus was measured as 1120.59 mm^2. These thickness values for cortical bone and cartilage are compatible within an acceptable range with the scientific literature reported for cortical bone [19–23] and articular cartilage [24–30]. Two standard M4 X 35 size malleolar screws were used for the fixation of the fracture fragments modelling. To obtain a realistic deformation behaviour of the fracture fixation, the threads of the screws were modelled with original design details. The buttress thread form with pitch of 1.75 mm, leading and trailing flank angles of 45° and 7° was used for the screw teeth form [31,32]. The solid modelling operation details and localisation of the double screw fixation of the fracture fragments are illustrated in Figure 1.

(**Figure 1.** The solid modelling operation details and localisation of the double screw fixation of the fracture fragments)

2.1.2. Material Properties

The literature related to FEA of bone structures was carefully conducted and deformation behaviour of the bone structures against assigned material properties given in related research was carefully evaluated. Although an agreement on specific material properties for bone structures could not be found, considering material modelling limitations, some experimental studies did provide helpful information related to material properties to be used in the numerical analysis. Additionally, in this study, pre-work FEA was solved against different material properties values to obtain logical deformation behaviour under defined boundary conditions. Finally, it was decided to assign material properties of cortical, trabecular and cartilage tissues separately since the cortical bone is denser and stronger than the porous trabecular structure. Assigning isotropic homogenous linear elastic material model definitions for all components utilised in the simulation study detailed in this paper would satisfactorily serve the study's primary aim. The material properties were selected from previous literature, which provides primarily experimental research results. Material properties assigned in the FEA setup are given in Table 2 [33–41].

(**Table 2.** Material properties assigned in the FEA setup)

2.1.3. Boundary Conditions

Loading magnitude was calculated considering the subject's weight (98 kg). The loading scenarios assumed that the patient was standing on his right leg just after the fracture fixation operation and the ankle joint was axially (vertical) loaded during this single leg static stance through fibula and tibia. Although it is known that muscles and other soft tissues also support the fibula and tibia against body weight, the main load is taken by these two bone columns. Based on experimental research reported by Wang *et al* (1996), the human tibia and fibula share the axial loading magnitude with the ratio of 84.3 % and 15.7 %, respectively [42]. Hence, the loading magnitude on the tibia structure was assigned in the FEA setup as 810.44 N, which corresponds to the patient weight of 98 kg. Another boundary condition parameter, which influences the simulation results, is the contact definitions between components included in a FEA. Detailed frictional contact (nonlinear contact) definitions between fracture fragments, screws, and the tibia–talus cartilage components were considered in this simulation study. Bonded contact definitions for the cartilage belonging to the tibia and talus bones were separately defined as an anatomical reality. Herewith, 24 contact (pairs) definitions within the tibia-talus assembly model used in the FEA setup were separately described (Figure 2). Stiffness and penetration tolerance between contact pairs were assigned as automatic program controlled in the FEA software and average penetration between base and fracture contact pairs were calculated as 1.36×10^{-4} mm. Some research in the literature related to FEA of tibial bone fracture screw/implant fixation operations does not utilise the screw preload [14,43–46]. The opposite to this approach, in real-life clinical operations, preload on the screw is applied to tighten the fracture fragments and this conveniently applied preload force makes a positive contribution to the healing period of the fracture zone. Application of screw preload would also play a critical role in the deformation behaviour of the fixed fragments. Therefore, the screw preload effect was considered in this study and preload of 2.5 N was defined to simulate the realistic displacement of the fixed fragments and screw performance [47]. In the simulation scenarios, the tibia-talus assembly model was bordered within Ø 65 x 88 mm cylindrical volume extracted from the full ankle joint and the structure loaded axially (vertical) via a titanium alloy (Ti-6Al-4V) compressive plate (Ø 35 x 5 mm). The plate was only allowed to make an axial (vertical) free movement. Its radial and horizontal movements were restricted to axially transferring the applied load to the bone structure. To reduce the physical solution time, the half talus bone modelling was used (a similar modelling approach was reported by Klekiel and Będziński (2015)) and its flat bottom faces were fixed [40]. On account of the pure loading analysis assumption, standard earth gravitational force was not defined in the simulation. Illustration of the boundary conditions, screw preload magnitude and coefficients of friction assigned in the simulation are given in Figure 2 and Table 3, respectively [47–51].

(**Figure 2.** Illustration of the boundary conditions and contact details assigned in the simulation scenarios)

(**Table 3.** Coefficients of friction and fixation screw preload assigned in the FEA set up)

2.1.4. Mesh Structure

Employing experimental validation and verification studies specific to FEM may be helpful; however, experimental validations may not be available for all kinds of studies. Experimental validation is planned for future research activity and is therefore not in the scope of research activity detailed in this paper; however, FE model verification was carried out through both mesh density (sensitivity) analysis and skewness metric (mesh quality) checks for the FEA utilised in this research.

A mesh sensitivity check is a determiner in the decision of appropriate element size. Specific to this study, the loading scenario of the healthy tibia-talus structure was employed for the mesh sensitivity analysis (as this was the solid base model) with various element sizes and identical boundary conditions as described previously. The effect of the different element size (from coarse to fine) on the maximum equivalent stress outputs of the tibia cortical bone structure was investigated. A constant element size for talus components and the compressive plate was assigned as 2 mm and the element sizes from 6 mm to 0.75 mm for tibia components were analysed. Thus, 10 different mesh configurations were analysed in this procedure. The results of the mesh sensitivity study indicated that the minimum element size was 1 mm in order to sufficiently represent the tibia bone structures (cortical and trabecular components) with an acceptable computation time. Additionally, one of the primary quality measures for a mesh structure in an FEA is the Skewness metric [52,53]. In addition to mesh sensitivity analysis, an element skewness check was conducted on the FE models with a decided element size of 1 mm. The average skewness values for healthy tibia and fixation loading scenarios were calculated as 0.22 and 0.24 respectivelly. These values indicated that the FE model used in the loading scenarios has an excellent mesh quality. Finally, an identical curvature meshing strategy was utilised in creating final FE models (mesh structures) of the solid models used in the simulations. Details of the mesh sensitivity analysis, skewness check and final FE model mesh structure are given in Figure 3.

(**Figure 3**. Details of the mesh sensitivity analysis (a), skewness check and final FE model mesh structure (b))

2.1.5. Solving Operation and Post-Processor Outputs

Simulation scenarios for no fracture (healthy tibia) and fracture fixation scenarios were run separately with identical boundary conditions after completion of the pre-processor steps and then visual and numerical outputs were recorded. The solving platform was a Dell Precision M4800 Series (Intel Core™ i7-4910MQ CPU @ 2.90GHz, NVIDIA Quadro K2100M-2GB, and Physical Memory: 32 GB) mobile workstation. Physical solution time was approximately 6 hours for each of the simulation scenarios of the fracture fixation.

2.2. Assumptions on Interfragmentary Micromotion and Fracture Healing

Previous studies have shown that if the gap within the fracture interface is less than 100 µm and interfragmentary strain is less than 2%, the fracture unites through primary bone healing [54–56]. For this reason, 100 µm displacement was accepted as the upper (critical) limit for primary fracture healing in this study.

2.3. Reliability of Fracture Angle Measurements

‘Medial malleolar fracture angle’ was defined as the angle of the fracture plane with the distal tibial articular surface in the coronal plane (Figure 1). Since this is a new angle measurement that is not used in clinical practice, the interobserver of this new measurement method has been tested. The institutional clinical database was retrospectively reviewed, and all patients with ankle fractures who had been admitted to Antalya Training and Research Hospital (Antalya, Turkey) between 2015 and December 2019 were identified. The anteroposterior ankle radiographs were obtained from the picture archiving and communication systems (PACS). Among these radiographs, 30 anteroposterior ankle radiographs with different types of fractures (transverse, oblique and vertical) were randomly selected and used for the reliability analysis. Two orthopaedic trauma surgeons performed the measurements. Observers were deliberately kept separate to each other’s recordings. Interobserver reliability was calculated using the interclass correlation coefficient (ICC) and a 95% confidence interval. Interpretation of the results was performed according to the scoring system suggested by Koo and Li (2016) (excellent >0.90, good 0.90–0.75, moderate 0.75-0.50 and poor <0.50) [57]. There were ten male and 20 female patients with a mean age of 41.4 ± 15.8 years (range, 14-65). The mean measurements performed by each observer were statistically similar (Observer A 46.3° ± 27.2° and Observer B 46.4° ± 4.8°, p=0.79). The inter-observer reliability was excellent, with an ICC of 0.995 (95%CI, 0.989-0.998).

3. RESULTS

Simulation results provided the magnitudes of maximum separation and sliding distance between fracture fragments. Additionally, equivalent (von Mises) stress and total body deformation distributions on the tibia components, the contact pressure between tibia and talus cartilages, frictional stress and contact pressure between fracture fragments were obtained. Related to these results, sample visual printout (FEA-000 and FEA-009) and numerical outputs are given in Figures 4 and Table 4, respectively (the simulation visual printouts of the 14 scenarios obtained from the FEA results are provided in supplementary files 1 and 2, respectively).

(**Figure 4.** FEA Results)

(**Table 4.** Numerical results obtained from FEA)

4. DISCUSSION

4.1. Interpretation of the FEA outputs

Concerning the loading direction (vertical, Y-axis), deformation results revealed that maximum displacements were 0.30 mm and 0.34 mm for no-fracture structure (FEA-000) and fracture fixation scenarios (at FEA-001; θ: 30°) respectively. The average axial displacement of all fracture fixation scenarios was 0.31 ± 0.01 mm under 810.44 N loading. These deformation results indicated that the directional displacement of the fractured structures was coherent with each other and logically in union with no-fracture loading resulting. Additionally, an increase in axial displacement (in µm scale) was observed at fracture angles of 30° and 35°. Above these angles, the axial displacement magnitudes were relatively close and coherent to no-fracture structure displacement. The reason for this may be explained as the sliding distance was more effective than the separation between fractured fragments in these fracture angles (θ: 30° and θ: 35°) in loading that causes higher axial displacement relatively; however, these directional displacement magnitudes of the whole structure would not be a reason for any damaging results under the predefined loading conditions.

Signs of damage can also be evaluated through stress distribution on the components by comparing the material's damage threshold such as ultimate or yield stress point (depending on material). In the fixation operation, the major load-bearing element is the screws. Maximum equivalent (von Mises) stress on the fixation screws was 87.61 MPa on the fractured structure with a fracture angle of 30°. This magnitude showed that the screws were approximately nine times safer (yield stress point: 795 MPa) in the fixation operations defined in this study. Maximum equivalent stress was calculated as 20.34 MPa on the tibia cortical for a no-fracture structure. The stress magnitudes of 19.73 MPa and 16.87 MPa on the tibia cortical base for fractured structures with a fracture angle of 30° and 90° were observed. Although the absolute difference between stress magnitudes at different fracture angles were relatively small in this component, a decrease was observed in incremental fracture angles in loading scenarios. The stress magnitudes obtained for the tibia cortical (for both base and fracture fragments) at different fracture angles indicated that the tibia cortical did not experience any damage compared to the cortical bone yield point of 111 MPa reported by Dong *et al.* (2012), with a factor of safety of approximately five [37].

Maximum equivalent (von Mises) stresses on the tibia trabecular bone were 1.03 MPa and 14.85 MPa for no-fracture structures and fractured base fragment with fracture angle of 35°, respectively. The maximum stress values varied from 9.78 MPa to 14.85 MPa on the fractured base fragments between fracture angles of 30° and 90°. The strength distribution pattern of tibia trabecular bone reported in related literature varies. Morgan *et al.* (2018) reported that the strength of the trabecular bone ranged between 0.1 and 30 MPa [58]. According to the experimental study reported by Jensen *et al.* (1988), maximum yield stress was measured as 18 MPa in their experiments [59]. Additionally, it was reported that the ultimate strength for the tibia medial malleoli had a mean value of 10.5 MPa (range 6.7-40 MPa) in front, and 7.3 MPa (range 1.3-41 MPa) behind. Ding *et al.* (1997) and Sierpowska *et al.* (2005) reported a value close to these mean values (reported yield stress is approximately 9 MPa) [25,60]. In this regard, the analysis results revealed a magnitude over 9 MPa, which may indicate that there is damage at the locations of the stress; however, when focused on the maximum stress locations (at the base and fractured fragments) on the trabecular bone, the stress intensity was evident at the very narrow points of screw teeth corners and the screw contact surfaces. This indicated that even small local damage was seen on these locations but would not affect the healing of fractured fragments after fixation operations as the sharp corners (such as screw teeth or narrow corners of fracture fragments) in loading may respond to an ignorable stress intensity which is a very common phenomenon in an FEA.

From evaluating cartilage damage under the pre-defined loading scenarios, the FEA revealed the maximum equivalent stresses of 1.31 MPa and 1.02 MPa on the tibia cartilage (base fragment) for no-fracture and the fractured structure with fracture angle of 90°, respectively. The average stress magnitude for the fixation loading scenarios was 0.82 ±0.07 MPa. Related literature reports that the strength necessary to cause damage of the articular cartilage varies between 4 MPa and 27 MPa [40,61,62]. In this regard, it was shown that the stress values obtained from the FEA did not show any damage on the cartilage component. Similarly, the average pressure measured on the cartilage contact surface between the tibia and talus were quite small values on static stance relative to gait, and interpreted as Park *et al.* (2018) reported peak contact pressure of the talus cartilage was 6.6 MPa at the 1st peak, 5.9 MPa at midstance, and 8.8 MPa at the second peak during gait [63]. The average contact pressures were 0.67 MPa and 0.77 MPa for no-fracture and fractured structure with fracture angle of 30° respectively in this FEA study. The average contact pressure for fixation loading scenarios was calculated as 0.75 ±0.01 MPa. Here, a relative increase in contact pressure for fracture fixation loading scenarios was clear compared to a no-fracture loading case as the contact surface area is smaller at the fractured base fragments under identical loading magnitudes.

The results extracted from the FEA revealed beneficial visual and numerical outputs for the displacement behaviour of the MM fracture fragments, which is the main focus of this study requiring clarification. The separation and sliding behaviour of the fragments under pre-defined boundary conditions were clearly exhibited in Figure 4 and the supplementary files. Numerical results emphasise the increase in separation through incrementation of the fracture angle. However, a decrease in sliding distance was observed and relative numerical variation was not as effective in sliding as in the fragment separation response. Minimum and maximum separation distance were 3.75 µm and 150.34 µm between fracture fragments at fracture angles of 30° and 90°, respectively. Minimum and maximum sliding distances were 25.87 µm and 41.37 µm between fracture fragments at fracture angle of 90° and 35°, respectively.

Contact pressure and frictional stress between MM fracture fragments were also extracted from the FEA. The numerical results obtained from the FEA revealed a similar pattern for the contact pressure and the frictional stress through incrementation of the fracture angle. An increase in these parameters was seen between fracture angles of 30° and 65°, however, above 65°, these parameters had lower magnitudes. Maximum contact pressure and maximum frictional stress between the fracture fragments were obtained at the fracture angle of 65° as 4.57 MPa and 2.10 MPa, respectively.

The decrease in these parameters after a specific point is understandable as the separation magnitude is increasing while sliding distance is decreasing, that would cause a lower contact interaction effect between the fragments. This also supports the decision of the critical fracture angle in double screw fixation operations.

4.2. Clinical Implications

This study aimed to determine the effect of the fracture angle on the stability of screw fixation in MM fractures. The results showed that more than 100 µm displacement occurs after the obliquity of fracture exceeds 70°. Based on these assumptions, a vertical MM fracture may be defined as a fracture between 70° to 90°. Secondly, two cancellous lag screws inserted perpendicular to the fracture plane can be adequate for MM fractures between 30° to 70°, without disturbing the mechanobiology of the fracture healing even after single-leg axial loading.

This information has significant implications in the classification of MM fractures. Herscovici classification system categorises the MM fractures based on subjective descriptions without providing objective thresholds to accurately assign a fracture to a group. From this point of view, the findings in this current study may guide the modifications or development of new classification systems. Secondly, the measurement of the fracture angle is easy and highly reproducible. It can be considered that ankle fractures occur in similar patterns and can be easily classified. However, 13 subgroups in Lauge-Hansen (1950) and 27 AO/OTA classification subgroups were described. In addition, atypical ankle fractures that cannot be classified with these systems have also been reported [7,64], because the resultant pattern of the fracture varies according to the position of the foot, direction and magnitude of the deforming force and quality of the bone. Thus, it may not be a proper approach to limit these into simply transverse, oblique, or vertical fractures without offering an angular value to separate these fracture patterns.

The second important clinical implication of the findings in this study is on the planning of the treatment. In general, anti-glade plate fixation is advocated for a vertical MM fracture, whereas two cancellous or cortical screws are said to be adequate for oblique MM fractures. Similarly, no objective criteria are presented in these treatment recommendations to distinguish between vertical and oblique fractures. Based on these findings, it may be claimed that surgeons should prefer plate fixation if the coronal fracture angle exceeds 70°. Finally, these findings may also guide the rehabilitation and weight-bearing schedule after MM fracture fixation. In the case of an isolated MM fracture with less than 70° fracture angle, early weight-bearing may be allowed if the fracture is fixed with two cancellous screws.

Few biomechanical studies compare fixation techniques in vertical MM fractures. In their cadaver study, Toolan *et al*. (1994) found that two lag screws provide a stronger fixation than the buttress plate fixation. However, they inserted a single screw close to the apex of the fracture over plate [65]. Dumigan *et al.* (2006) found that when two distal and proximal screws were added to the buttress plate, the most durable construct was formed compared to screw-only fixations [12]. In this study, sliding displacement did not significantly change as the fracture obliquity increased. In other words, there were no distinct differences in sliding distance between 30° and 90° fractures.

On the contrary, as the angle of fracture increased, the apex of the fracture acted as a pivot point, and the articular separation steadily increased. It could be considered that a stronger fixation close to the articular level would prevent displacement. This phenomenon is also supported by the findings in the study conducted by Amanatullah *et al.* (2012) and Wegner *et al.* (2016) [13,66]. Amanatullah *et al.* (2012) compared different screw configurations (parallel, convergent and divergent) in vertical MM fractures and reported that divergent screw fixation was the strongest construct. In a similar study by Wegner *et al.* (2016), bi-cortical screws eliminated the separation of the fracture more than uni-cortical screws in similar loadings. Based on these previous reports and the findings in this current study, the separation of the fracture fragments at the articular level decreases as the strength of the fixation increases.

There is only one study in current literature similar to this that examines MM fractures using FEA. Jiang *et al.* (2019) modelled 30°, 60° and 90° MM fractures and tested their self-designed anatomic plate and screw configurations on these models [14]. They reported that plate fixation caused the least displacement with 300 N, 500 N and 700 N abduction loading in each fracture angle. The displacements obtained in that study differ from this study, being approximately ten times larger. There are multiple reasons for this discrepancy. First, the loading of the model is entirely different. Second, while Jiang *et al.* (2019) loaded the model directly over MM and up to 700 N, loading was performed through the talus in this study, which is a more realistic scenario [14]. Besides, the material properties used during modelling were also different. Comparing all these studies with each other may not provide logical inferences due to many differences such as study designs, tested configurations, materials used and modelling.

4.3. Limitations Regarding Material Model and the FEA

In real-life applications, based on experimental evidence, bone structures exhibit viscoelastic behaviour under deformation [67]. The behaviour of the bone material is time-dependent and the viscoelastic behaviour is highly nonlinear. This type of nonlinear viscoelastic behaviour is normally classified as viscoplasticity, which is a time-dependent plasticity phenomenon [68]. It is also known that the bone structures are anisotropic, non-homogeneous and that advancing age, menopause, or metabolic diseases related to mineral homeostasis affect the remodelling process of bone and consequently alter behaviour under loading [69].

Nonlinear viscoelastic behaviour of the bone structures is a very complex phenomenon. Therefore, in order to explain the viscoelastic behaviour of the bone structures, researchers are forced to make simplifying assumptions and apply the theories of linear viscoelasticity or Hookean elasticity in biomechanical analyses. The nonlinear viscoelastic material model was not considered in this research as it would be difficult and impractical to determine/simulate permanent (plastic) deformation (which is the main reason for the tissue bruising) case. However, solid structure damage can be determined more easily by considering the critical stress point (ultimate or yield stress points) defined for the numerical model as the damage behaviour of bone structures corresponds to the generation of microcracks over the yield stress point [58]. Additionally, any real material that shows deviation from the ideal material models and numerical method-based simulation tools still has some limitations in modelling real-life responses. Therefore, appropriate assumptions should be made with respect to the material properties and the purpose of the simulation study.

Another important issue related to nonlinear material models used in a FEA is the loading rate, which obviously affects the bone deformation characteristics. However, Hambli (2013) and Morgan *et al.* (2018) indicate that rate-dependent effects have a moderate impact on physiological strain rates of the bone structures as they occur during normal daily activities [58,70]. Hence, in the low strain rate loading regimes, bone viscosity and material nonlinearity can be neglected under the consideration of pre-defined boundary conditions. Scientific literature also supports that in the static loading cases, homogeneous isotropic material model assumptions provide acceptable results when compared to an inhomogeneous anisotropic material model [70].

It must also be emphasised that the literature related to the determination of material properties of the bone structures cannot provide any standards or full agreement for the critical material properties to be used in the numerical method-based analysis such as FEA. Some research related to FEA of bone structures assumes the trabecular and cortical structures to be separated; however, others assume them to be a single body and provide different values for each material's mechanical properties such as modulus of elasticity, Poisson's ratio, yield stress, density etc. For example, some studies provide the modulus of elasticity (as one of the critical mechanical properties) as 7.30 GPa; however, Niu *et al.* (2013) reports that this value is a bit lower than experimental results given by other literature which provide the value between 13.10 GPa and 32.20 GPa for the modulus of elasticity of human tibia [71]. Wirtz *et al.* (2000), Cammarata *et al.* (2016) and a detailed review on bone properties by Novitskaya *et al.* (2011) report this disagreement (changing values) on the material properties (most especially on modulus of elasticity) of human bones given in the literature [72–74]. It was also reported that different material testing methods (such as tensile, compression and bending tests) might provide different ranges for the material properties of bone structures [75]. Similarly, Morgan *et al.* (2018) reports that the typical elastic modulus of human trabecular bone ranges between 10 and 3000 MPa [58]. In this study, material properties of cortical, trabecular and cartilage tissues are separately assigned with an assumption of isotropic homogenous linear elastic material model. Although nonlinear viscoplastic material model might represent more realistic results, the simulation outputs revealed that numerical and visual results reasonably reflected the deformation behaviour of the components under pre-defined boundary conditions.

Anatomically, the foot is a complex structure containing 26 bones, 33 joints, 107 ligaments, and 33 muscles, nearly 25 % of all human bones [40]. The study focused on the medial malleolus fracture double screw fixation on tibia bone; therefore, the other components connected to the ankle joint such as fibula bone, ligaments, muscles, other inner tissues and the skin were not considered in the FEA utilised in this research. Thus, it avoided potential limitations and barriers for the major aim of this study, which might be experienced during modelling, simulation set up and solving operations. This was the major limitation in creating an FEA set up in this study, which forced the simplification of assumptions in describing the model geometry and boundary condition operations. In this study, the double screw fixation operation of the MM fracture with various fracture angles was analysed by means of FEA, which is a numerical analysis technique that can approximate solutions. Errors in FEA are inevitable. These are mostly methodical and numerical errors and they may occur during the establishment of the mathematical model (e1), the mathematical discontinuity (e2) and the numerical solution processes (e3) [76–78]. In addition to these errors, user-based errors can occur during set up and interpretation of the FEA results, so this aspect should also be kept under consideration in the final evaluation stage, however, it is widely accepted in various scientific disciplines that FEA is a very useful analysis tool in order to simulate real-life loading conditions. Therefore, it can transmit significant information in order to improve or develop treatment techniques used in orthopaedic applications. In addition to the potential limitations discussed above, this study was limited with static stance loading conditions and linear elastic homogeneous isotropic material models. Dynamic conditions of the tibia loading after fixation operation which may be experienced during the gait or different loading conditions, should be evaluated. The effect of nonlinear and viscoelastic non-homogenous material behaviour should also be kept under consideration. Finally, the simulation results were re-checked to determine whether any errors (methodical, numerical or analysis based) might be experienced in the FEA of the tibia loading. The results are provided after carefully re-checking the operations and it was interpreted that the FEA was setup using acceptable assumptions and gave accurate and logical outputs under pre-defined boundary conditions considered in this research.

4.4. Limitations Regarding the Clinical Reality

First, with a real fracture, the fracture plane is not a flat surface, but rather a surface with several interdigitations and this microstructure provides friction and additional stiffness to the total construct. After an ankle fracture operation, patients are usually not allowed any weight-bearing activity for the first 3-4 weeks. However, this research has examined an immediate weight-bearing scenario to understand early weight-bearing and whether quicker rehabilitation is feasible.

During the first three weeks, the fracture would start healing, and a considerable amount of callus would be formed. This would also increase the stiffness of the construct. Furthermore, all soft tissues, including tendons, muscles and ligaments that may displace or stabilise the fracture, were all ignored. Another limitation concerns the maximum amount of movement for the healing of a fracture. This research has accepted 100 µm, which is also reported in the literature, but there are clinical studies reporting that MM fractures heal up to 2 mm displacement [2].

5. CONCLUSIONS

The main purpose of this study was to provide a clear understanding of the angular discrimination between oblique and vertical MM fractures though visual and numerical outputs and, in this regard, to guide surgeons in the decision making procedures for critical fracture angle in related surgeries. To do this, an advanced engineering simulation approach including geometric and contact nonlinearity was utilised in the study. As the principal conclusion, screw fixation perpendicular to the direction of a MM fracture with more than 70° angle with the tibial plafond results in a significant articular separation (> 100 µm) during a single-leg stand. Below this critical angle, two screws provide sufficient fixation, hence, it can be concluded that two screw fixation would be sufficiently utilised at the fracture angles from 30° to 70°. Based on the findings in this study, a vertical and oblique fracture definition may be performed, which will ease the classification of these fractures and the treatment algorithms may be rearranged. However, these data should be supported by clinical studies in practice. In a MM fracture which has more than 70° angle, from a structural stability point of view, three screw fixation may be considered most appropriate as it may provide a smaller deflection under loading. However, this operation procedure should be tested with smaller screw dimensions in order to avoid any crack propagation in screw driving zones, that may cause undesired bone fractures during or after the fixation operation. Additionally, it may require more than just screws to stabilise the fracture, and in this case, fixation may be achieved using a narrow metal plate (such as a buttress plate) with screws situated on both sides of the fracture line. In addition to these conclusions, this study provides a well-described FEA design study and a useful 'how-to-do' strategy for informing further research on complicated stress and deformation analyses of medial malleolus fractures through advanced engineering simulation techniques.

Acknowledgement

This research was partly supported financially by The Scientific Research Projects Coordination Unit of Akdeniz University (Antalya-Turkey) and Antalya Training and Research Hospital (Antalya-Turkey). The authors declare that they have no known competing financial interests or personal relationships that could have appeared to influence the work reported in this paper.

References

1. Elsoe R, Ostgaard SE, Larsen P. Population-based epidemiology of 9767 ankle fractures. *Foot Ankle Surg* 2018; 24: 34–39.
2. Herscovici D, Scaduto JM, Infante A. Conservative treatment of isolated fractures of the medial malleolus. *J Bone Joint Surg Br* 2007; 89-B: 89–93.
3. Ebraheim NA, Ludwig T, Weston JT, et al. Comparison of surgical techniques of 111 medial malleolar fractures classified by fracture geometry. *Foot Ankle Int* 2014; 35: 471–477.
4. Hanhisuanto S, Kortekangas T, Pakarinen H, et al. The functional outcome and quality of life after treatment of isolated medial malleolar fractures. *Foot Ankle Surg* 2017; 23: 225–229.
5. Tan EW, Sirisreetreerux N, Paez AG, et al. Early Weightbearing After Operatively Treated Ankle Fractures. *Foot Ankle Int* 2016; 37: 652–658.
6. Lampridis V, Gougoulias N, Sakellariou A. Stability in ankle fractures: Diagnosis and treatment. *EFORT Open Rev* 2018; 3: 294–303.
7. Lauge-Hansen N. Fractures of the ankle. II. Combined experimental-surgical and experimental-roentgenologic investigations. *Arch Surg* 1950; 60: 957–985.
8. Müller ME, Koch P, Nazarian S, et al. *The Comprehensive Classification of Fractures of Long Bones*. Springer Berlin Heidelberg, 1990. Epub ahead of print 1990. DOI: 10.1007/978-3-642-61261-9.
9. Collinge C, Dombroski D, Heier K. Ankle Fractures and Dislocations. In: Stannard JP, Schmidt AH (eds) *Surgical Treatment of Orthopaedic Trauma*. Stuttgart: Georg Thieme Verlag. Epub ahead of print 29 January 2016. DOI: 10.1055/b-0036-129630.
10. Ebraheim NA, Weston JT, Ludwig T, et al. The association between medial malleolar fracture geometry, injury mechanism, and syndesmotic disruption. *Foot Ankle Surg* 2014; 20: 276–280.
11. Aitken SA, Johnston I, Jennings AC, et al. An evaluation of the Herscovici classification for fractures of the medial malleolus. *Foot Ankle Surg* 2017; 23: 317–320.
12. Dumigan RM, Bronson DG, Early JS. Analysis of Fixation Methods for Vertical Shear Fractures of the Medial Malleolus. *J Orthop Trauma* 2006; 20: 687–691.
13. Wegner AM, Wolinsky PR, Robbins MA, et al. Antiglide plating of vertical medial malleolus fractures provides stiffer initial fixation than bicortical or unicortical screw fixation. *Clin Biomech* 2016; 31: 29–32.
14. Jiang D, Zhan S, Wang Q, et al. Biomechanical Comparison of Locking Plate and Cancellous Screw Techniques in Medial Malleolar Fractures: A Finite Element Analysis. *J Foot Ankle Surg* 2019; 58: 1138–1144.
15. SolidWorks Product. SolidWorks Product Release 2019 SP5, www.solidworks.com (2019).
16. ANSYS Product. ANSYS Product Release 2019 R.2, www.ansys.com (2019).
17. 3D Slicer Product. 3D Slicer Product Release 4.10.2, https://www.slicer.org/ (2019).
18. Autodesk Meshmixer Product. Autodesk Meshmixer Product Release 2019. *Autodesk Inc.*, https://www.meshmixer.com/ (2019, accessed 25 September 2020).

19. Bolliger Neto R, Rossi JD, Leivas TP. Experimental determination of bone cortex holding power of orthopedic screw. *Rev Hosp Clin Fac Med Sao Paulo* 1999; 54: 181–186.

20. Veitch SW, Findlay SC, Ingle BM, et al. Accuracy and precision of peripheral quantitative computed tomography measurements at the tibial metaphysis. *J Clin Densitom* 2004; 7: 209–217.

21. Mohammad SH, Hunter RL, Tatarski RL, et al. Assessing Cortical Thickness in Human Tibiae With Sonography vs Computed Tomography: A Pilot Study. *J Diagnostic Med Sonogr* 2018; 34: 170–179.

22. Du W, Zhang J, Hu J. A Method to determine cortical bone thickness of human femur and tibia using clinical ct scans. In: *Conference proceedings International Research Council on the Biomechanics of Injury, IRCOBI*. 2018, pp. 388–398.

23. Vogl F, Patil M, Taylor WR. Sensitivity of low-frequency axial transmission acoustics to axially and azimuthally varying cortical thickness: A phantom-based study. *PLoS One* 2019; 14: e0219360.

24. Shepherd DET, Seedhom BB. Thickness of human articular cartilage in joints of the lower limb. *Ann Rheum Dis* 1999; 58: 27–34.

25. Ding M, Dalstra M, Danielsen CC, et al. AGE VARIATIONS IN THE PROPERTIES OF HUMAN TIBIAL TRABECULAR BONE. *J Bone Joint Surg Br* 1997; 79-B: 995–1002.

26. Sugimoto K, Takakura Y, Tohno Y, et al. Cartilage thickness of the talar dome. *Arthrosc - J Arthrosc Relat Surg* 2005; 21: 401–404.

27. Wan L, de Asla RJ, Rubash HE, et al. Determination of in-vivo articular cartilage contact areas of human talocrural joint under weightbearing conditions. *Osteoarthr Cartil* 2006; 14: 1294–1301.

28. Millington SA, Grabner M, Wozelka R, et al. Quantification of ankle articular cartilage topography and thickness using a high resolution stereophotography system. *Osteoarthr Cartil* 2007; 15: 205–211.

29. Maier J, Black M, Bonaretti S, et al. Comparison of Different Approaches for Measuring Tibial Cartilage Thickness. *J Integr Bioinform*; 14. Epub ahead of print 28 July 2017. DOI: 10.1515/jib-2017-0015.

30. Kim J. *The Effect of Bone and Ligament Morphology of Ankle Joint Loading in the Neutral Position*. Old Dominion University. Epub ahead of print 1 July 2017. DOI: 10.25777/rvqt-0e42.

31. Weinstein RB. Orthopedic screw mechanics. (Chapter 36). The podiatry institute, pp. 184–190.

32. Stahel PF, Alfonso NA, Henderson C, et al. Introducing the 'Bone-Screw-Fastener' for improved screw fixation in orthopedic surgery: A revolutionary paradigm shift? *Patient Saf Surg* 2017; 11: 6.

33. Oldani C, Dominguez A. Titanium as a Biomaterial for Implants. In: *Recent Advances in Arthroplasty*. InTech, 2012. Epub ahead of print 27 January 2012. DOI: 10.5772/27413.

34. Alonso-Rasgado T, Jimenez-Cruz D, Karski M. 3-D computer modelling of malunited posterior malleolar fractures: Effect of fragment size and offset on ankle stability, contact pressure and pattern. *J Foot Ankle Res* 2017; 10: 13.

35. Anderson DD, Goldsworthy JK, Li W, et al. Physical validation of a patient-specific contact finite element model of the ankle. *J Biomech* 2007; 40: 1662–1669.

36. Zhu ZJ, Zhu Y, Liu JF, et al. Posterolateral ankle ligament injuries affect ankle stability: A finite element study.

BMC Musculoskelet Disord 2016; 17: 96.

37. Dong XN, Acuna RL, Luo Q, et al. Orientation dependence of progressive post-yield behavior of human cortical bone in compression. *J Biomech* 2012; 45: 2829–2834.

38. Wang X, Nyman JS, Dong X, et al. Fundamental Biomechanics in Bone Tissue Engineering. *Synth Lect Tissue Eng* 2010; 2: 1–225.

39. Kim SH, Chang SH, Jung HJ. The finite element analysis of a fractured tibia applied by composite bone plates considering contact conditions and time-varying properties of curing tissues. *Compos Struct* 2010; 92: 2109–2118.

40. Klekiel T, Będziński R. Finite element analysis of large deformation of articular cartilage in upper ankle joint of occupant in military vehicles during explosion. *Arch Metall Mater* 2015; 60: 2115–2121.

41. Novitskaya E, Zin C, Chang N, et al. Creep of trabecular bone from the human proximal tibia. *Mater Sci Eng C* 2014; 40: 219–227.

42. Wang Q, Whittle M, Cunningham J, et al. Fibula and its ligaments in load transmission and ankle joint stability. *Clin Orthop Relat Res* 1996; 261–270.

43. Huang X, Zhi Z, Yu B, et al. Stress and stability of plate-screw fixation and screw fixation in the treatment of Schatzker type IV medial tibial plateau fracture: A comparative finite element study. *J Orthop Surg Res* 2015; 10: 182.

44. Oken OF, Yildirim AO, Asilturk M. Finite element analysis of the stability of AO/OTA 43-C1 type distal tibial fractures treated with distal tibia medial anatomic plate versus anterolateral anatomic plate. *Acta Orthop Traumatol Turc* 2017; 51: 404–408.

45. Cao Y, Zhang Y, Huang L, et al. The impact of plate length, fibula integrity and plate placement on tibial shaft fixation stability: A finite element study. *J Orthop Surg Res* 2019; 14: 52.

46. Chen F, Huang X, Ya Y, et al. Finite element analysis of intramedullary nailing and double locking plate for treating extra-articular proximal tibial fractures. *J Orthop Surg Res* 2018; 13: 12.

47. Marvan J, Horak Z, Vilimek M, et al. Fixation of distal fibular fractures: A biomechanical study of plate fixation techniques. *Acta Bioeng Biomech* 2017; 19: 33–39.

48. Hayden LR, Escaro S, Wilhite DR, et al. A Comparison of Friction Measurements of Intact Articular Cartilage in Contact with Cartilage, Glass, and Metal. *J Biomimetics, Biomater Biomed Eng* 2019; 41: 23–35.

49. Gao X, Fraulob M, Haïat G. Biomechanical behaviours of the bone-implant interface: A review. *Journal of the Royal Society Interface*; 16. Epub ahead of print 2019. DOI: 10.1098/rsif.2019.0259.

50. Hayes WC, Perren SM. Plate-bone friction in the compression fixation of fractures. *Clin Orthop Relat Res* 1972; 89: 236–240.

51. Eberle S, Gerber C, Von Oldenburg G, et al. A biomechanical evaluation of orthopaedic implants for hip fractures by finite element analysis and in-vitro tests. *Proc Inst Mech Eng Part H J Eng Med* 2010; 224: 1141–1152.

52. Brys G, Hubert M, Struyf A. A robust measure of skewness. *J Comput Graph Stat* 2004; 13: 996–1017.

53. ANSYS Product Doc. ANSYS Meshing User's Guide: Skewness (Release 2019 R2). *ANSYS Inc., USA.*, https://ansyshelp.ansys.com/account/secured?returnurl=/Views/Secured/corp/v191/wb2_help/wb2_help.html (2019, accessed 25 September 2020).

54. Shapiro F. Cortical bone repair: The relationship of the lacunar-canalicular system and intercellular gap junctions to the repair process. *J Bone Jt Surg - Ser A* 1988; 70: 1067–1081.

55. Blecha LD, Zambelli PY, Ramaniraka NA, et al. How plate positioning impacts the biomechanics of the open wedge tibial osteotomy; A finite element analysis. *Comput Methods Biomech Biomed Engin* 2005; 8: 307–313.

56. Shimamura Y, Kaneko K, Kume K, et al. The initial safe range of motion of the ankle joint after three methods of internal fixation of simulated fractures of the medial malleolus. *Clin Biomech* 2006; 21: 617–622.

57. Koo TK, Li MY. A Guideline of Selecting and Reporting Intraclass Correlation Coefficients for Reliability Research. *J Chiropr Med* 2016; 15: 155–163.

58. Morgan EF, Unnikrisnan GU, Hussein AI. Bone Mechanical Properties in Healthy and Diseased States. *Annu Rev Biomed Eng* 2018; 20: 119–143.

59. Jensen NC, Hvid I, Krøner K. Strength Pattern of Cancellous Bone at the Ankle Joint. *Eng Med* 1988; 17: 71–76.

60. Sierpowska J, Hakulinen MA, Töyräs J, et al. Prediction of mechanical properties of human trabecular bone by electrical measurements. In: *Physiological Measurement*. IOP Publishing, p. S119.

61. Klekiel T, Wodzisławski J, Będziński R. Modelling of Damping Properties of Articular Cartilage During Impact Load. *Eng Trans* 2017; 65: 133–145.

62. Raju M, Siva Rama Krishna L, Haroon A, et al. Analysis of Ankle Joint with Articular Cartilage. *Int J Creat Res Thoughts* 2018; 6: 288–293.

63. Park S, Lee S, Yoon J, et al. Finite element analysis of knee and ankle joint during gait based on motion analysis. *Med Eng Phys* 2019; 63: 33–41.

64. Kose O, Yuksel HY, Guler F, et al. Isolated Adult Tillaux Fracture Associated With Volkmann Fracture—A Unique Combination of Injuries: Report of Two Cases and Review of the Literature. *J Foot Ankle Surg* 2016; 55: 1057–1062.

65. Toolan BC, Koval KJ, Kummer FJ, et al. Vertical shear fractures of the medial malleolus: A biomechanical study of five internal fixation techniques. *Foot Ankle Int* 1994; 15: 483–489.

66. Amanatullah DF, Khan SN, Curtiss S, et al. Effect of divergent screw fixation in vertical medial malleolus fractures. *J Trauma Acute Care Surg* 2012; 72: 751–754.

67. Wu Z, Ovaert TC, Niebur GL. Viscoelastic properties of human cortical bone tissue depend on gender and elastic modulus. *J Orthop Res* 2012; 30: 693–699.

68. LeMaitre J. Introduction to Viscoplasticity. In: *Handbook of Materials Behavior Models*. Elsevier, 2001, pp. 301–302.

69. Yamashita J, Li X, Furman BR, et al. Collagen and bone viscoelasticity: A dynamic mechanical analysis. *J Biomed Mater Res* 2002; 63: 31–36.

70. Hambli R. A quasi-brittle continuum damage finite element model of the human proximal femur based on element deletion. *Med Biol Eng Comput* 2013; 51: 219–231.

71. Niu WX, Wang LJ, Feng TN, et al. Effects of bone Young's modulus on finite element analysis in the lateral ankle biomechanics. *Appl Bionics Biomech* 2013; 10: 189–195.

72. Wirtz DC, Schiffers N, Forst R, et al. Critical evaluation of known bone material properties to realize anisotropic FE-simulation of the proximal femur. *J Biomech* 2000; 33: 1325–1330.

73. Cammarata M, Nicoletti F, Di Paola M, et al. Mechanical behavior of human bones with different saturation levels. Montreal, QC.: 2nd International Electronic Conference on Materials (MDPI AG), 2016, p. B003.

74. Novitskaya E, Chen P-Y, Hamed E, et al. Recent advances on the measurement and calculation of the elastic moduli of cortical and trabecular bone: A review. *Theor Appl Mech* 2011; 38: 209–297.

75. Khan S, Warkhedkar R, Shyam A. Human Bone strength Evaluation through different Mechanical Tests. *Res Artic Int J Curr Eng Technol*. Epub ahead of print 2014. DOI: 10.14741/ijcet/spl.2.2014.102.

76. Salmi S. Multidisciplinary Design Optimization in an Integrated CAD / FEM Environment. 2008; 81.

77. Narasaiah GL. *Finite Element Analysis*. B.S. Publications, https://www.biblio.com/9788178001401 (2008, accessed 25 September 2020).

78. Pancoast D. *Solidworks Simulation-2010 Training Manual*. PMT1040-EN ed. Dassault System - Solidworks Corporation, 2009.

Table Captions

Table 1. List of the FEA scenarios

Table 2. Material properties assigned in the FEA setup

Table 3. Coefficients of friction and fixation screw preload assigned in the FEA set up

Table 4. Numerical results obtained from FEA

Figure Captions

Figure 1. The solid modelling operation details and localisation of the double screw fixation of the fracture fragments

Figure 2. Illustration of the boundary conditions and contact details assigned in the simulation scenarios

Figure 3. Details of the mesh sensitivity analysis (a), skewness check and final FE model mesh structure (b)

Figure 4. FEA Results

Table 1. List of the FEA scenarios

FEA Scenario Code	Description of the FEA Scenarios	FEA Scenario Code	Description of the FEA Scenarios
FEA-000	Healty Tibia / No fracture	FEA-007	2 x M 4 mm Malleolar Screw Fixation / Fracture Angle: 60 °
FEA-001	2 x M 4 mm Malleolar Screw Fixation / Fracture Angle: 30 °	FEA-008	2 x M 4 mm Malleolar Screw Fixation / Fracture Angle: 65 °
FEA-002	2 x M 4 mm Malleolar Screw Fixation / Fracture Angle: 35 °	FEA-009	2 x M 4 mm Malleolar Screw Fixation / Fracture Angle: 70 °
FEA-003	2 x M 4 mm Malleolar Screw Fixation / Fracture Angle: 40 °	FEA-010	2 x M 4 mm Malleolar Screw Fixation / Fracture Angle: 75 °
FEA-004	2 x M 4 mm Malleolar Screw Fixation / Fracture Angle: 45 °	FEA-011	2 x M 4 mm Malleolar Screw Fixation / Fracture Angle: 80 °
FEA-005	2 x M 4 mm Malleolar Screw Fixation / Fracture Angle: 50 °	FEA-012	2 x M 4 mm Malleolar Screw Fixation / Fracture Angle: 85 °
FEA-006	2 x M 4 mm Malleolar Screw Fixation / Fracture Angle: 55 °	FEA-013	2 x M 4 mm Malleolar Screw Fixation / Fracture Angle: 90 °

Table 2. Material properties assigned in the FEA setup

Homogenous isotropic linear elastic material model

Parameters	Unit	Model Components			
		Cortical Bone	Trabecular Bone	Cartilage	Fixation Screw (M4 x 35) (Ti-6Al-4V)
Modulus of Elasticity	(MPa)	19100 [e,f]	1000.61 [g,h]	12 [b,c,d]	115000 [a]
Poisson's Ratio	(-)	0.30 [b]	0.30 [b]	0.42 [c,d]	0.33 [a]
Density	($kg\ m^{-3}$)	1980 [b]	830 [i]	431 [b]	4500 [a]

a. Oldani and Dominguez (2012)
b. Alonso-Rasgado et al (2017)
c. Andersona et al (2007)
d. Zhu et al (2016)
e. Dong et al (2012)
f. Wang et al (2010)
g. Kim et al (2010)
h. Klekiel and Będziński (2015)
i. Novitskaya et al (2014)

Table 3. Coefficients of friction and fixation screw preload assigned in the FEA set up

Parameters	Components in Relation	Value
Coefficient of Friction between	Cartilage and Cartilage	0.0164 [a]
	Bony Parts and Fixation Screw	0.37 [b,c]
	Bony Parts	0.46 [d]
Fixation Screw Preload [e] (N)	.	2.5

a. Hayden et al (2019)
b. Gao et al (2019)
c. Hayes and Perren (1972)
d. Eberle et al (2010)
e. Marvan et al (2017)

Table 4. Numerical results obtained from FEA

FEA Study Code	Fracture Angle	Max. Separation (Gap)	Max. Sliding Distance	Contact Pressure between Base and Fracture Fragments	Frictional Stress between Base and Fracture Fragments	Average Contact Pressure on Cartilage Surface between Tibia and Talus (Base Surface)	Max. Eq. Stress by Components						Max. Directional Displacement
							Tibia Cortical - Base Fragment	Tibia Cortical - Fracture Fragment	Tibia Trabecular - Base Fragment	Tibia Trabecular - Fracture Fragment	Tibia Cartilage - Base Fragment	Fixation Screws	Total (Y-Axis)
	(◦)	(µm)	(µm)	(MPa)	(MPa)	(MPa)	(MPa)	(MPa)	(MPa)	(MPa)	(MPa)	(MPa)	(mm)
FEA - 000	No Fracture	No Fracture	No Fracture	No Fracture	No Fracture	0.67	**20.34**	No Fracture	1.03	No Fracture	**1.31**	No Fracture	0.30
FEA - 001	30	3.75	38.13	1.43	0.66	**0.77**	19.73	14.96	10.84	11.25	0.79	**87.61**	**0.34**
FEA - 002	35	4.82	**41.37**	1.50	0.69	0.76	19.21	12.23	**14.85**	**11.73**	0.77	82.17	0.34
FEA - 003	40	9.15	35.07	1.70	0.78	0.75	19.31	15.16	11.92	11.31	0.79	60.21	0.31
FEA - 004	45	15.35	36.48	2.43	1.12	0.75	19.26	9.63	12.49	10.71	0.77	73.65	0.31
FEA - 005	50	19.28	35.27	2.61	1.20	0.75	19.08	11.28	12.25	10.11	0.79	79.71	0.30
FEA - 006	55	26.97	36.51	3.09	1.47	0.75	18.96	14.50	12.36	9.42	0.77	75.92	0.31
FEA - 007	60	36.81	36.29	3.46	1.59	0.75	18.85	12.23	12.32	8.83	0.81	81.30	0.31
FEA - 008	65	58.08	35.67	**4.57**	**2.10**	0.74	18.60	14.27	12.51	8.04	0.77	83.00	0.30
FEA - 009	70	78.95	36.39	4.31	1.98	0.74	18.02	14.86	13.04	6.82	0.84	82.04	0.30
FEA - 010	75	109.09	33.36	3.34	1.53	0.75	17.73	11.66	12.39	4.92	0.89	86.80	0.30
FEA - 011	80	116.47	32.08	2.09	0.96	0.75	17.34	9.02	11.96	4.23	0.84	85.69	0.30
FEA - 012	85	119.88	30.98	1.93	0.89	0.74	17.12	11.43	10.97	3.45	0.87	80.30	0.30
FEA - 013	90	**150.34**	25.87	0.92	0.42	0.75	16.87	**15.81**	9.78	4.35	1.02	77.55	0.30

Indicates maximum values

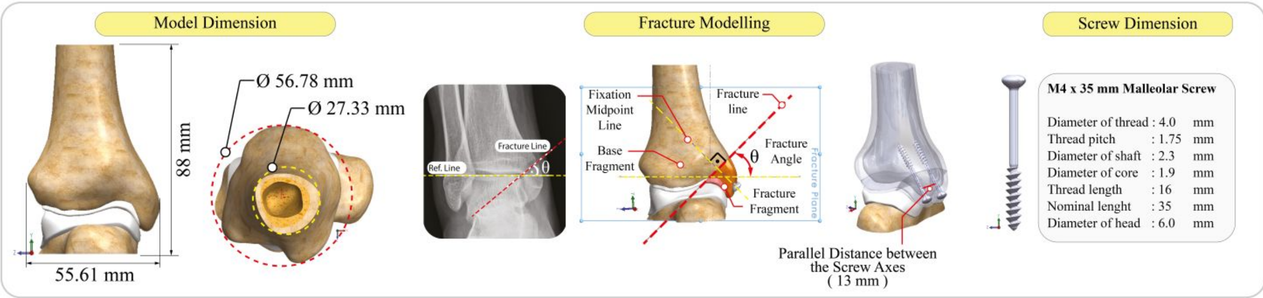

(**Figure 1.** The solid modelling operation details and localisation of the double screw fixation of the fracture fragments)

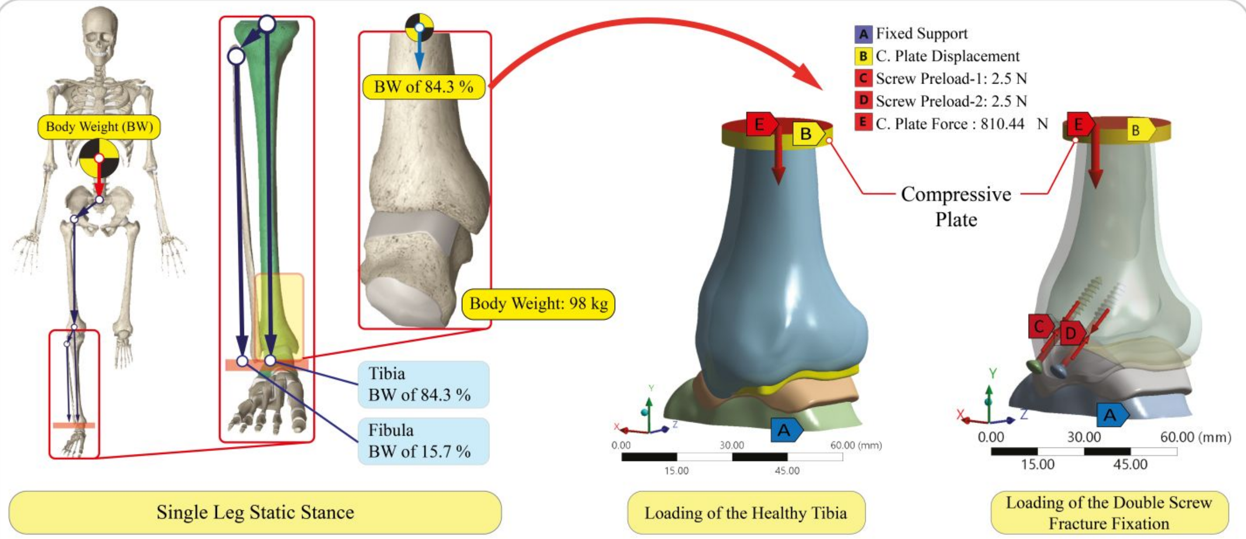

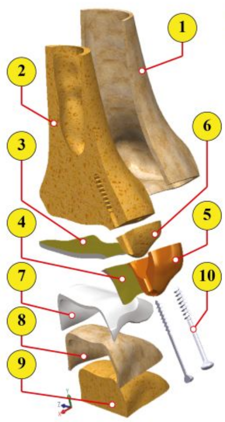

Model Components

1. Base Fragment: Tibia Cortical
2. Base Fragment: Tibia Trabecular
3. Base Fragment: Tibia Cartilage
4. Fracture Fragment: Tibia Cartilage
5. Fracture Fragment: Tibia Cortical
6. Fracture Fragment: Tibia Trabecular
7. Talus Cartilage
8. Talus Cortical
9. Talus Trabecular
10. Malleolar Screw (M4 x 35 mm)

Contact No	Related Components in the Contact Pairs: Contact Bodies	Related Components in the Contact Pairs: Target Bodies	Contact Definition in the FEA
1	Talus Cartilage	Talus Cortical	BONDED
2	Talus Cortical	Talus Trabecular	BONDED
3	Compressive Plate	Tibia Trabecular - Base Fragment	BONDED
4	Tibia Cortical - Base Fragment	Tibia Cartilage - Base Fragment	BONDED
5	Compressive Plate	Tibia Cortical - Base Fragment	BONDED
6	Tibia Cortical - Fracture Fragment	Tibia Trabecular - Fracture Fragment	BONDED
7	Tibia Cortical - Fracture Fragment	Tibia Cartilage - Fracture Fragment	BONDED
8	Tibia Cortical - Fracture Fragment	Talus Cartilage	FRICTIONAL
9	Tibia Cartilage - Base Fragment	Talus Cartilage	FRICTIONAL
10	Tibia Cartilage - Fracture Fragment	Talus Cartilage	FRICTIONAL
11	Tibia Trabecular - Base Fragment	Tibia Cortical - Base Fragment	FRICTIONAL
12	Tibia Trabecular - Base Fragment	Tibia Trabecular - Fracture Fragment	FRICTIONAL
13	Tibia Trabecular - Base Fragment	Tibia Cortical - Fracture Fragment	FRICTIONAL
14	Tibia Cortical - Base Fragment	Tibia Trabecular - Fracture Fragment	FRICTIONAL
15	Tibia Cortical - Base Fragment	Tibia Cortical - Fracture Fragment	FRICTIONAL
16	Tibia Cortical - Base Fragment	Tibia Cartilage - Fracture Fragment	FRICTIONAL
17	Tibia Cartilage - Base Fragment	Tibia Cortical - Fracture Fragment	FRICTIONAL
18	Tibia Cartilage - Base Fragment	Tibia Cartilage - Fracture Fragment	FRICTIONAL
19	Tibia Trabecular - Base Fragment	C. Screw-1	FRICTIONAL
20	Tibia Trabecular - Base Fragment	C. Screw-2	FRICTIONAL
21	Tibia Trabecular - Fracture Fragment	C. Screw-1	FRICTIONAL
22	Tibia Trabecular - Fracture Fragment	C. Screw-2	FRICTIONAL
23	Tibia Cortical - Fracture Fragment	C. Screw-1	FRICTIONAL
24	Tibia Cortical - Fracture Fragment	C. Screw-2	FRICTIONAL

Figure 2. Illustration of the boundary conditions and contact details assigned in the simulation scenarios

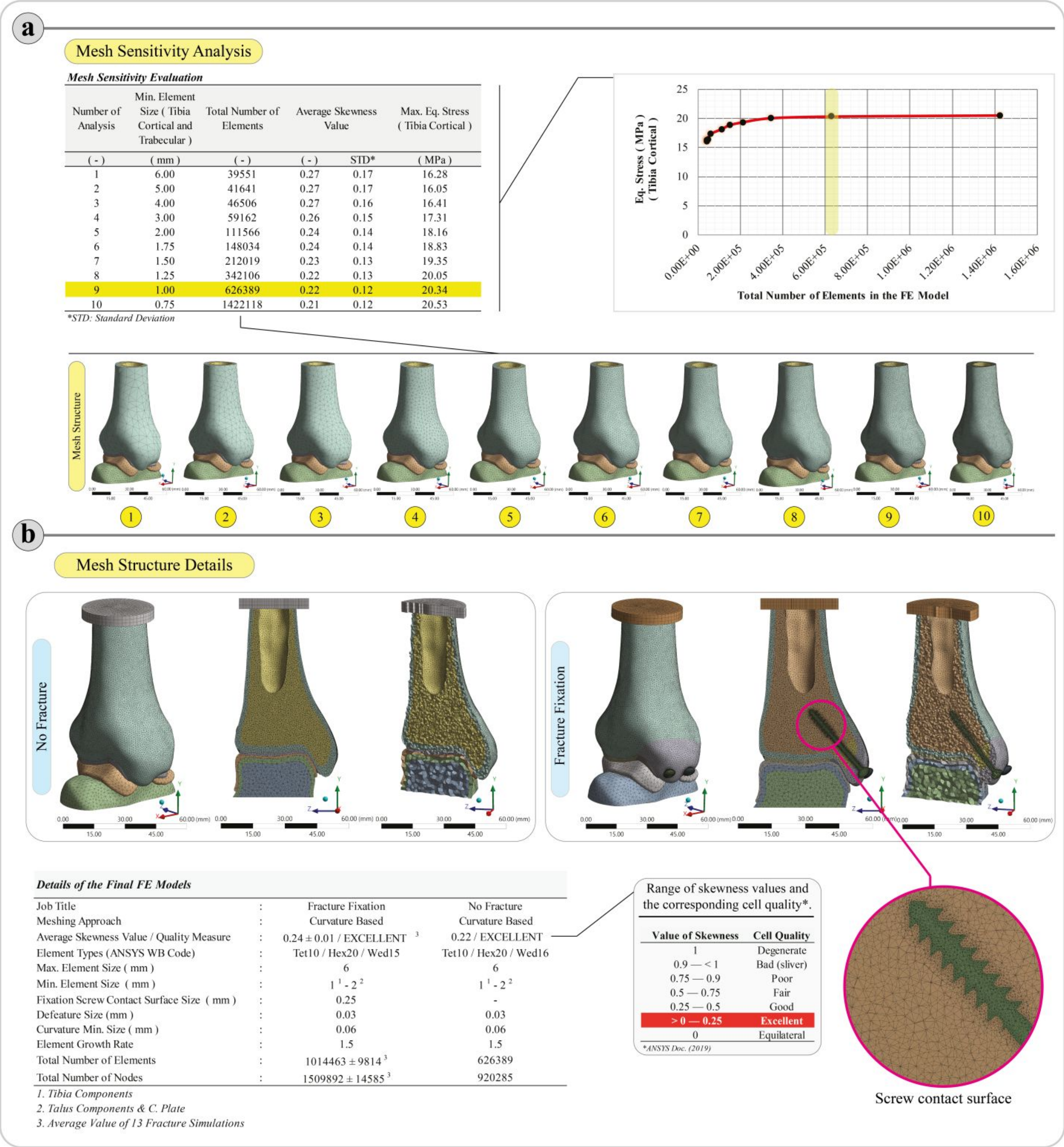

Mesh Sensitivity Evaluation

Number of Analysis	Min. Element Size (Tibia Cortical and Trabecular)	Total Number of Elements	Average Skewness Value		Max. Eq. Stress (Tibia Cortical)
(-)	(mm)	(-)	(-)	STD*	(MPa)
1	6.00	39551	0.27	0.17	16.28
2	5.00	41641	0.27	0.17	16.05
3	4.00	46506	0.27	0.16	16.41
4	3.00	59162	0.26	0.15	17.31
5	2.00	111566	0.24	0.14	18.16
6	1.75	148034	0.24	0.14	18.83
7	1.50	212019	0.23	0.13	19.35
8	1.25	342106	0.22	0.13	20.05
9	1.00	626389	0.22	0.12	20.34
10	0.75	1422118	0.21	0.12	20.53

**STD: Standard Deviation*

Details of the Final FE Models

Job Title	:	Fracture Fixation	No Fracture
Meshing Approach	:	Curvature Based	Curvature Based
Average Skewness Value / Quality Measure	:	0.24 ± 0.01 / EXCELLENT [3]	0.22 / EXCELLENT
Element Types (ANSYS WB Code)	:	Tet10 / Hex20 / Wed15	Tet10 / Hex20 / Wed16
Max. Element Size (mm)	:	6	6
Min. Element Size (mm)	:	1 [1] - 2 [2]	1 [1] - 2 [2]
Fixation Screw Contact Surface Size (mm)	:	0.25	-
Defeature Size (mm)	:	0.03	0.03
Curvature Min. Size (mm)	:	0.06	0.06
Element Growth Rate	:	1.5	1.5
Total Number of Elements	:	1014463 ± 9814 [3]	626389
Total Number of Nodes	:	1509892 ± 14585 [3]	920285

1. Tibia Components
2. Talus Components & C. Plate
3. Average Value of 13 Fracture Simulations

Range of skewness values and the corresponding cell quality*.

Value of Skewness	Cell Quality
1	Degenerate
0.9 — < 1	Bad (sliver)
0.75 — 0.9	Poor
0.5 — 0.75	Fair
0.25 — 0.5	Good
> 0 — 0.25	Excellent
0	Equilateral

**ANSYS Doc. (2019)*

Figure 3. Details of the mesh sensitivity analysis (a), skewness check and final FE model mesh structure (b)

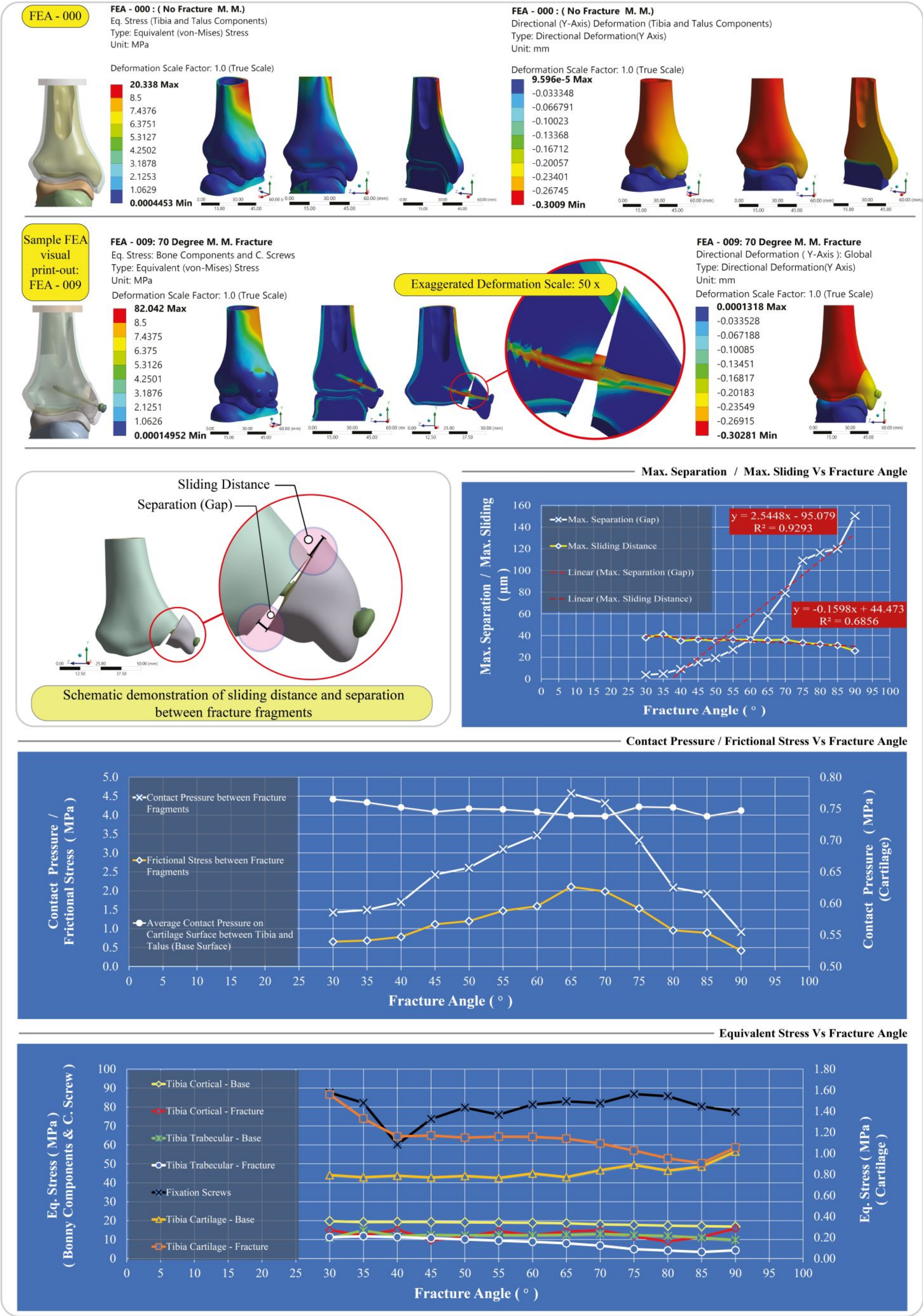

Figure 4. FEA Results

SUPPLEMENTARY - 1 of 2
FEA Results
Visual print-outs

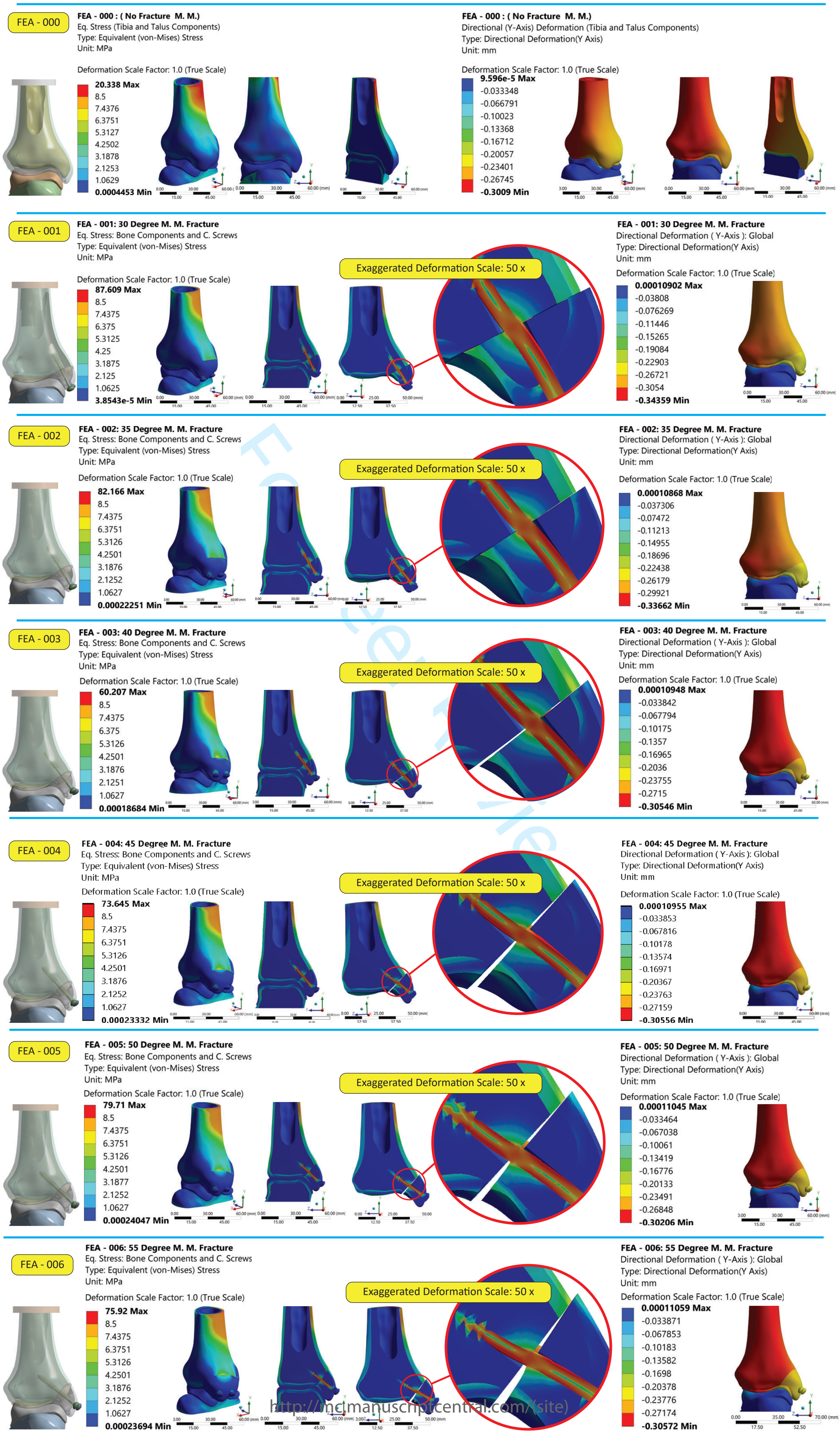

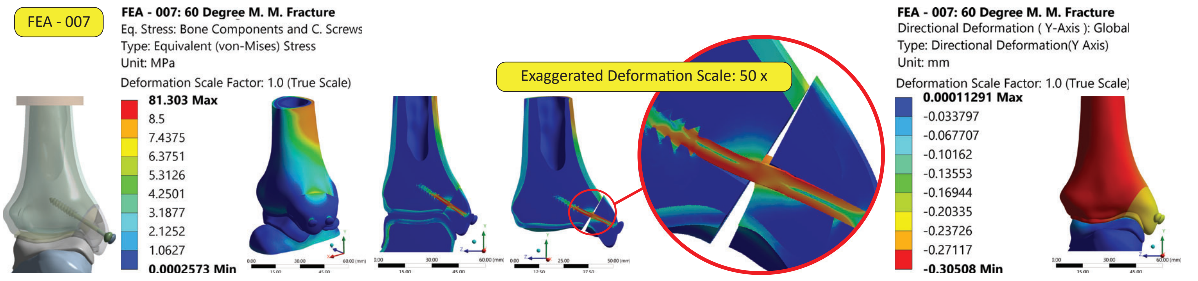
FEA - 007
FEA - 007: 60 Degree M. M. Fracture
Eq. Stress: Bone Components and C. Screws
Type: Equivalent (von-Mises) Stress
Unit: MPa
Deformation Scale Factor: 1.0 (True Scale)
81.303 Max
8.5
7.4375
6.3751
5.3126
4.2501
3.1877
2.1252
1.0627
0.0002573 Min
Exaggerated Deformation Scale: 50 x
FEA - 007: 60 Degree M. M. Fracture
Directional Deformation (Y-Axis): Global
Type: Directional Deformation(Y Axis)
Unit: mm
Deformation Scale Factor: 1.0 (True Scale)
0.00011291 Max
-0.033797
-0.067707
-0.10162
-0.13553
-0.16944
-0.20335
-0.23726
-0.27117
-0.30508 Min

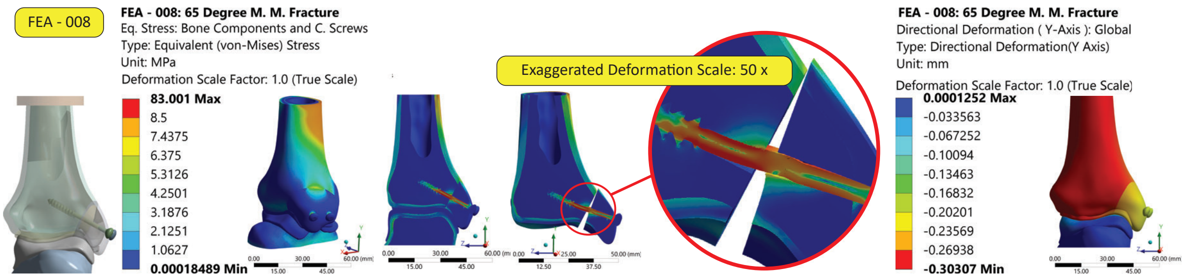
FEA - 008
FEA - 008: 65 Degree M. M. Fracture
Eq. Stress: Bone Components and C. Screws
Type: Equivalent (von-Mises) Stress
Unit: MPa
Deformation Scale Factor: 1.0 (True Scale)
83.001 Max
8.5
7.4375
6.375
5.3126
4.2501
3.1876
2.1251
1.0627
0.00018489 Min
Exaggerated Deformation Scale: 50 x
FEA - 008: 65 Degree M. M. Fracture
Directional Deformation (Y-Axis): Global
Type: Directional Deformation(Y Axis)
Unit: mm
Deformation Scale Factor: 1.0 (True Scale)
0.0001252 Max
-0.033563
-0.067252
-0.10094
-0.13463
-0.16832
-0.20201
-0.23569
-0.26938
-0.30307 Min

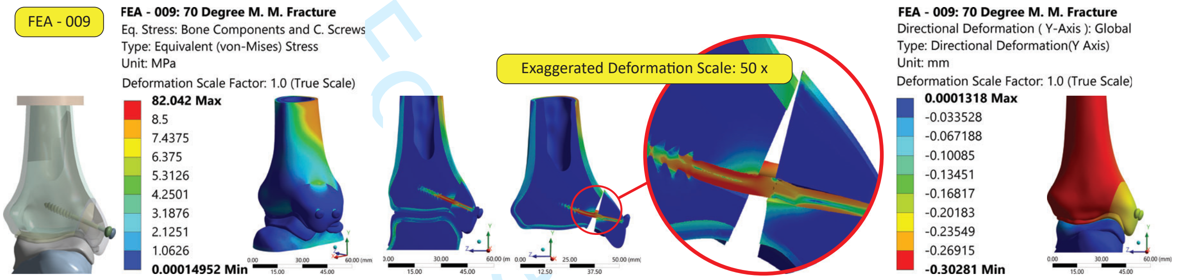
FEA - 009
FEA - 009: 70 Degree M. M. Fracture
Eq. Stress: Bone Components and C. Screws
Type: Equivalent (von-Mises) Stress
Unit: MPa
Deformation Scale Factor: 1.0 (True Scale)
82.042 Max
8.5
7.4375
6.375
5.3126
4.2501
3.1876
2.1251
1.0626
0.00014952 Min
Exaggerated Deformation Scale: 50 x
FEA - 009: 70 Degree M. M. Fracture
Directional Deformation (Y-Axis): Global
Type: Directional Deformation(Y Axis)
Unit: mm
Deformation Scale Factor: 1.0 (True Scale)
0.0001318 Max
-0.033528
-0.067188
-0.10085
-0.13451
-0.16817
-0.20183
-0.23549
-0.26915
-0.30281 Min

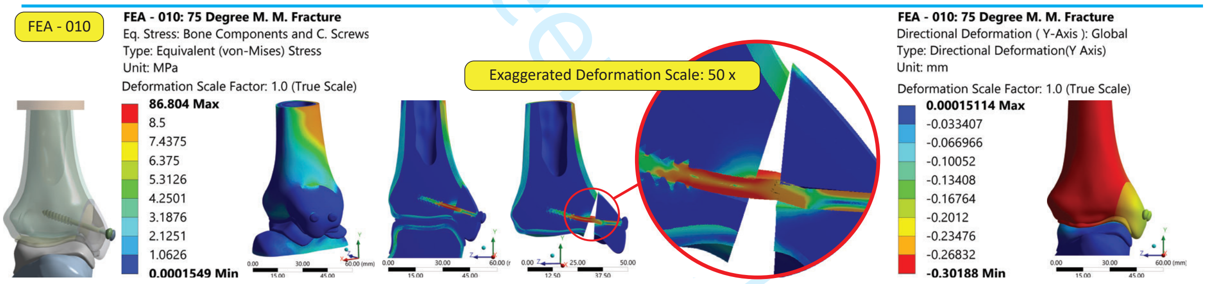
FEA - 010
FEA - 010: 75 Degree M. M. Fracture
Eq. Stress: Bone Components and C. Screws
Type: Equivalent (von-Mises) Stress
Unit: MPa
Deformation Scale Factor: 1.0 (True Scale)
86.804 Max
8.5
7.4375
6.375
5.3126
4.2501
3.1876
2.1251
1.0626
0.0001549 Min
Exaggerated Deformation Scale: 50 x
FEA - 010: 75 Degree M. M. Fracture
Directional Deformation (Y-Axis): Global
Type: Directional Deformation(Y Axis)
Unit: mm
Deformation Scale Factor: 1.0 (True Scale)
0.00015114 Max
-0.033407
-0.066966
-0.10052
-0.13408
-0.16764
-0.2012
-0.23476
-0.26832
-0.30188 Min

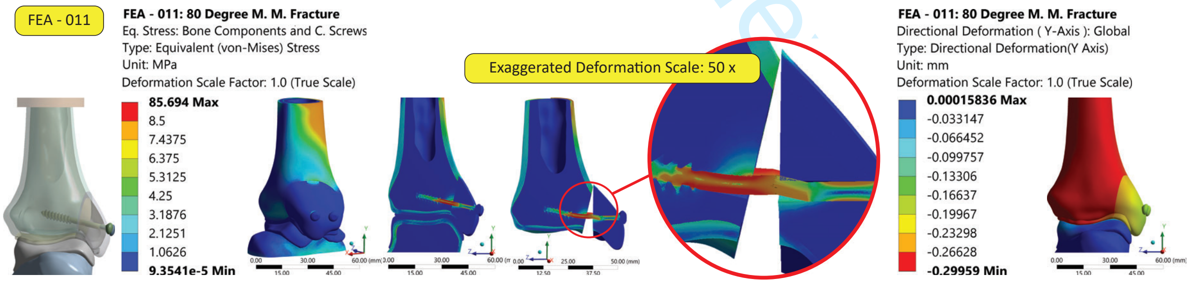
FEA - 011
FEA - 011: 80 Degree M. M. Fracture
Eq. Stress: Bone Components and C. Screws
Type: Equivalent (von-Mises) Stress
Unit: MPa
Deformation Scale Factor: 1.0 (True Scale)
85.694 Max
8.5
7.4375
6.375
5.3125
4.25
3.1876
2.1251
1.0626
9.3541e-5 Min
Exaggerated Deformation Scale: 50 x
FEA - 011: 80 Degree M. M. Fracture
Directional Deformation (Y-Axis): Global
Type: Directional Deformation(Y Axis)
Unit: mm
Deformation Scale Factor: 1.0 (True Scale)
0.00015836 Max
-0.033147
-0.066452
-0.099757
-0.13306
-0.16637
-0.19967
-0.23298
-0.26628
-0.29959 Min

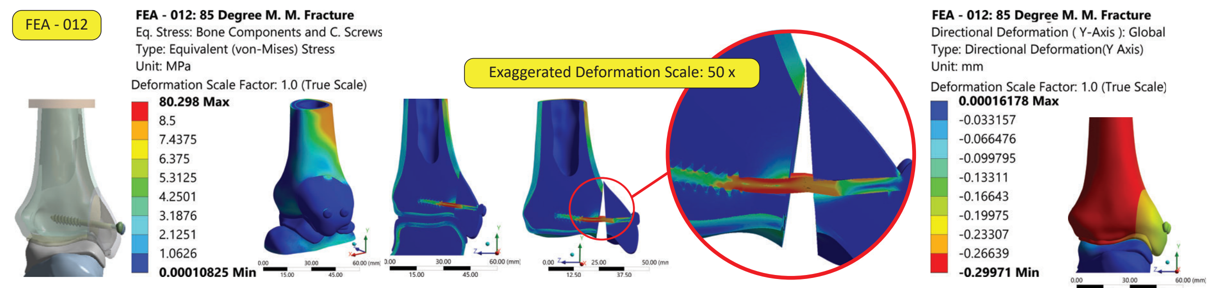
FEA - 012
FEA - 012: 85 Degree M. M. Fracture
Eq. Stress: Bone Components and C. Screws
Type: Equivalent (von-Mises) Stress
Unit: MPa
Deformation Scale Factor: 1.0 (True Scale)
80.298 Max
8.5
7.4375
6.375
5.3125
4.2501
3.1876
2.1251
1.0626
0.00010825 Min
Exaggerated Deformation Scale: 50 x
FEA - 012: 85 Degree M. M. Fracture
Directional Deformation (Y-Axis): Global
Type: Directional Deformation(Y Axis)
Unit: mm
Deformation Scale Factor: 1.0 (True Scale)
0.00016178 Max
-0.033157
-0.066476
-0.099795
-0.13311
-0.16643
-0.19975
-0.23307
-0.26639
-0.29971 Min

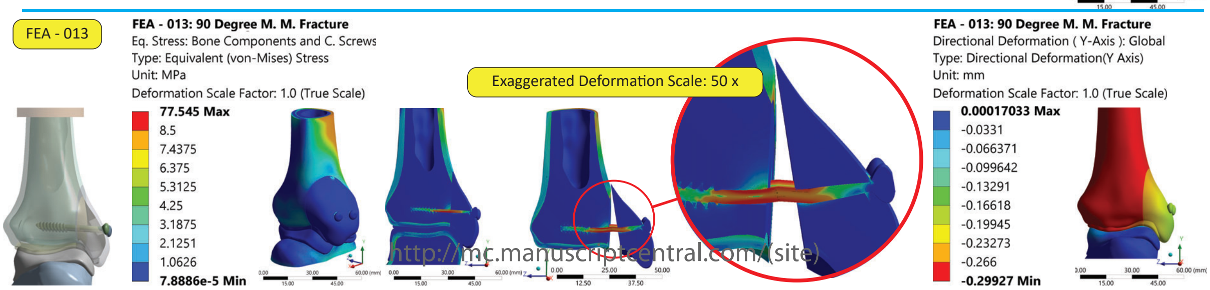
FEA - 013
FEA - 013: 90 Degree M. M. Fracture
Eq. Stress: Bone Components and C. Screws
Type: Equivalent (von-Mises) Stress
Unit: MPa
Deformation Scale Factor: 1.0 (True Scale)
77.545 Max
8.5
7.4375
6.375
5.3125
4.25
3.1875
2.1251
1.0626
7.8886e-5 Min
Exaggerated Deformation Scale: 50 x
FEA - 013: 90 Degree M. M. Fracture
Directional Deformation (Y-Axis): Global
Type: Directional Deformation(Y Axis)
Unit: mm
Deformation Scale Factor: 1.0 (True Scale)
0.00017033 Max
-0.0331
-0.066371
-0.099642
-0.13291
-0.16618
-0.19945
-0.23273
-0.266
-0.29927 Min

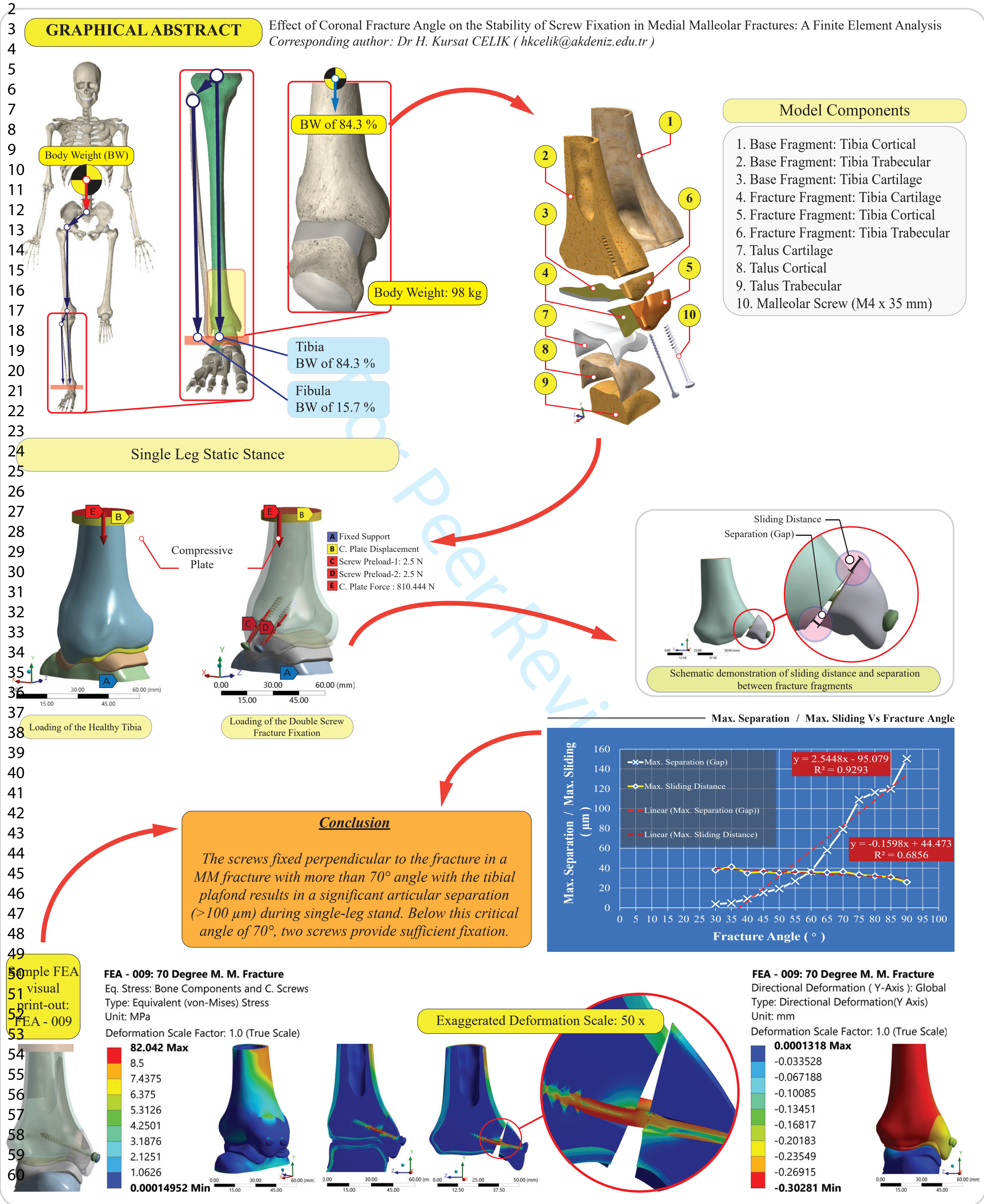
GRAPHICAL ABSTRACT
Effect of Coronal Fracture Angle on the Stability of Screw Fixation in Medial Malleolar Fractures: A Finite Element Analysis
Corresponding author: Dr H. Kursat CELIK (hkcelik@akdeniz.edu.tr)
Body Weight (BW)
BW of 84.3 %
Body Weight: 98 kg
Tibia
BW of 84.3 %
Fibula
BW of 15.7 %
Single Leg Static Stance
Model Components
1. Base Fragment: Tibia Cortical
2. Base Fragment: Tibia Trabecular
3. Base Fragment: Tibia Cartilage
4. Fracture Fragment: Tibia Cartilage
5. Fracture Fragment: Tibia Cortical
6. Fracture Fragment: Tibia Trabecular
7. Talus Cartilage
8. Talus Cortical
9. Talus Trabecular
10. Malleolar Screw (M4 x 35 mm)
Compressive Plate
A Fixed Support
B C. Plate Displacement
C Screw Preload-1: 2.5 N
D Screw Preload-2: 2.5 N
E C. Plate Force : 810.444 N
Loading of the Healthy Tibia
Loading of the Double Screw Fracture Fixation
Sliding Distance
Separation (Gap)
Schematic demonstration of sliding distance and separation between fracture fragments
Max. Separation / Max. Sliding Vs Fracture Angle
Max. Separation (Gap)
Max. Sliding Distance
Linear (Max. Separation (Gap))
Linear (Max. Sliding Distance)
y = 2.5448x - 95.079
R² = 0.9293
y = -0.1598x + 44.473
R² = 0.6856
Max. Separation / Max. Sliding (μm)
Fracture Angle (°)
Conclusion
The screws fixed perpendicular to the fracture in a MM fracture with more than 70° angle with the tibial plafond results in a significant articular separation (>100 μm) during single-leg stand. Below this critical angle of 70°, two screws provide sufficient fixation.
Sample FEA visual print-out: FEA - 009
FEA - 009: 70 Degree M. M. Fracture
Eq. Stress: Bone Components and C. Screws
Type: Equivalent (von-Mises) Stress
Unit: MPa
Deformation Scale Factor: 1.0 (True Scale)
82.042 Max
8.5
7.4375
6.375
5.3126
4.2501
3.1876
2.1251
1.0626
0.00014952 Min
Exaggerated Deformation Scale: 50 x
FEA - 009: 70 Degree M. M. Fracture
Directional Deformation (Y-Axis): Global
Type: Directional Deformation(Y Axis)
Unit: mm
Deformation Scale Factor: 1.0 (True Scale)
0.0001318 Max
-0.033528
-0.067188
-0.10085
-0.13451
-0.16817
-0.20183
-0.23549
-0.26915
-0.30281 Min